Downsizing of supermassive black holes from the SDSS quasar survey

M. Labita,[1]⋆ R. Decarli,[1] A. Treves[1] and R. Falomo[2]

[1]*Department of Physics and Mathematics, University of Insubria, Via Valleggio 11, I-22100 Como, Italy*
[2]*INAF, Astronomical Observatory of Padova, Vicolo dell'Osservatorio 5, I-35122 Padova, Italy*

ABSTRACT

Starting from the ∼50 000 quasars of the Sloan Digital Sky Survey for which Mg II line width and 3000 Å monochromatic flux are available, we aim to study the dependence of the mass of active black holes on redshift. We focus on the observed distribution in the full width at half-maximum–nuclear luminosity plane, which can be reproduced at all redshifts assuming a limiting M_{BH}, a maximum Eddington ratio and a minimum luminosity (due to the survey flux limit). We study the z-dependence of the best-fitting parameters of assumed distributions at increasing redshift and find that the maximum mass of the quasar population evolves as $\log(M_{BH(max)}/M_{\odot}) \sim 0.3z + 9$, while the maximum Eddington ratio (∼0.45) is practically independent of cosmic time. These results are unaffected by the Malmquist bias.

Key words: galaxies: active – galaxies: evolution – galaxies: nuclei – quasars: general.

1 INTRODUCTION

In the last years, a substantial effort has been devoted to measure black hole (BH) masses for various quasar samples covering a wide range of redshifts and luminosities. McLure & Dunlop (2004), from Hβ and Mg II, measured virial BH masses (M_{BH}) for ∼10 000 quasars with $z \leq 2.1$ included in the Sloan Digital Sky Survey (SDSS) Data Release 1 (DR1). Fine et al. (2006) used composite spectra to measure the dependence on redshift of the mean BH mass for an L^* subsample of the 2dF QSO Redshift Survey (2QZ) quasar catalogue (Croom et al. 2004) from $z \sim 0.5$ to 2.5. Shen et al. (2008) listed BH masses for ∼60 000 quasars in the redshift range $0.1 \lesssim z \lesssim 4.5$ contained in the SDSS DR5, by means of virial BH mass estimators based on the Hβ, Mg II and C IV lines.

A common result of these works is that the mean BH mass of the quasi-stellar object (QSO) population at given z appears to increase with redshift, but the observed z-dependence is dominated by the well-known Malmquist bias, because the BH mass strongly correlates with the central source luminosity (see Vestergaard et al. 2008 for a detailed analysis of the selection bias effects). McLure & Dunlop (2004), for instance, suggest that the observed active BH mass evolution is entirely due to the effective flux limit of the sample.

A full understanding of this scenario would give important insights on the BH formation and evolution and on the activation of the quasar phenomenon. Moreover, along with a parallel study on the dependence on redshift of the host galaxy luminosity (mass), this would enlighten on the joint evolution of galaxy bulges and their central BHs. For these reasons, it is of focal importance to trace the dependence of M_{BH} on z, overcoming the problems related to the Malmquist bias.

We start from the recently published SDSS DR5 quasar catalogue (Schneider et al. 2007) and focus on the ∼ 50 000 quasars for which Mg II line width and 3000 Å flux are available (Shen et al. 2008). The sample selection is described in Section 2. The sample ($0.35 < z < 2.25$) is divided in eight redshift bins, and it is shown that, in each bin, the object distribution in the full width at half-maximum (FWHM)–luminosity plane can be reproduced assuming a minimum luminosity, a maximum mass and a maximum Eddington ratio (Sections 3.2 and 3.3). Comparing the assumed probability density to the observed distribution of objects, the parameters can be determined in each redshift bin (Section 3.4). This procedure is shown to be unaffected by the Malmquist bias (Section 3.5), and provides a method to study the 'unbiased' dependence on redshift of quasar BH masses and Eddington ratios (Section 4.1). In Section 4.2, we test the dependence of our results on the assumed $r_{BLR} - \lambda L_\lambda$ calibration. We compare our results with the previous literature in Section 4.3, and in Section 4.4 we discuss some implications of our findings for the study of the co-evolution of supermassive BHs and their host galaxies. A summary of this paper is given in the last section.

Throughout this paper, we adopt a concordant cosmology with $H_0 = 70\,\mathrm{km\,s^{-1}\,Mpc^{-1}}$, $\Omega_m = 0.3$ and $\Omega_\Lambda = 0.7$.

2 THE MG II SAMPLE

The SDSS DR5 quasar catalogue (Schneider et al. 2007) contains more than 77 000 quasars. It covers about 8000 deg^2 and selects objects with $M_i < -22$, have at least one emission line with FWHM larger than 1000 km s^{-1} or are unambiguously broad-absorption-line objects, are fainter than $i = 15.0$ and have highly reliable redshifts.

Shen et al. (2008) calculated BH masses for ∼60 000 quasars in the redshift range $0.1 < z < 4.5$ included in the SDSS DR5

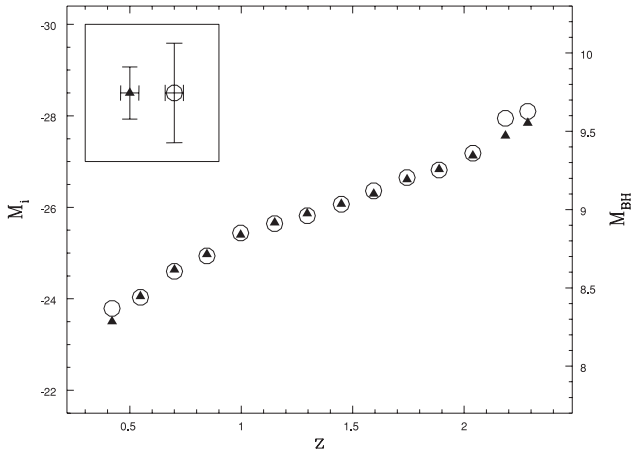⋆E-mail: marzia.labita@gmail.com

Figure 1. Average values of the absolute magnitude M_i (triangles) and of M_{BH} (circles) versus redshift, in bins $\Delta z = 0.15$. The typical standard deviation of each bin is given in the inset.

quasar catalogue, using virial BH mass estimators based on the Hβ, Mg II and C IV emission lines. They provide rest-frame line widths and monochromatic luminosities at 5100, 3000 and 1350 Å (see Shen et al. 2008 for details on calibrations, measure procedures and corrections).

In the following, we will focus on the $\sim 50\,000$ quasars from the Shen et al. (2008) sample for which Mg II line width and 3000 Å monochromatic flux are available (Mg II sample). We assume the virial theorem and adopt the calibration of McLure & Dunlop (2004) to evaluate the BH mass:

$$\log M_{BH} = 6 + \log(a) + 2\log(\text{FWHM}) + b \log \lambda L_\lambda \qquad (1)$$

with $a = 3.2 \pm 1.1$ and $b = 0.62 \pm 0.14$. Here, M_{BH} is expressed in solar masses, FWHM in units of 1000 km s^{-1} and λL_λ in units of $10^{44} \text{ erg s}^{-1}$.

3 DESCRIPTION OF THE PROCEDURE

3.1 Malmquist bias

Fig. 1 shows the mean absolute i magnitude (see Shen et al. 2008 for details) versus redshift of the Mg II sample. The effects of the Malmquist bias are apparent as an increase of the average observed luminosity with redshift. The mean BH mass versus redshift is over-plotted to the mean $M_i(z)$: it is apparent that the average observed BH masses follow the same trend as the absolute magnitudes with a higher dispersion, as expected given that the distribution of the line widths does not depend on luminosity or redshift (Shen et al. 2008). This suggests that the z-dependence of the observed BH masses is strongly subject to a Malmquist-type bias, because at high redshift one cannot observe low-mass objects. In order to trace the 'unbiased' dependence of active BH masses with redshift, one should consider a combination of two effects, namely the z-dependence of the quasar number density and the increase of the average mass of quasar populations with redshift. To illustrate these effects consider the following two extreme cases.

(i) The M_{BH} distribution does not depend on redshift, but the quasar number density increases until $z \sim 2$–2.5. At any redshift, there is a population of low-mass ($\sim 10^8 \text{ M}_\odot$) quasars, which cannot be observed at high redshift, and the population of high-mass ($\sim 10^{9.5} \text{ M}_\odot$) active BHs that is observed at $z \gtrsim 1.5$ is the high-mass end of the M_{BH} distribution.

(ii) The quasar M_{BH} distribution shifts towards higher masses at increasing redshift. The population of low-mass ($\sim 10^8 \text{ M}_\odot$) objects that is observed at low redshift is not present at all at $z \gtrsim 1.5$. The observed increase of M_{BH} with redshift, in active BHs, is 'true' and it is not due to a Malmquist-type bias.

Of course, each of these pictures is *per se* unlikely: the observed dependence on redshift of quasar BH masses is due to a combination of both these effects. In the following, we will concentrate on these points using statistical arguments, focusing on the distribution of objects in the FWHM–luminosity plane.

3.2 Quasar distribution in the FWHM–λL_λ plane

Fig. 2 shows the objects of the Mg II sample in the logFWHM–logλL_λ plane (see Fine et al. 2008 for a similar approach). The sample has been divided in eight redshift bins of equal comoving volume. In each panel, it is apparent that the data points form a sort of 'triangle', the left-hand side of which represents a cut due to the survey flux limit (which gives rise to the Malmquist bias). From equation (1), the loci of quasars with constant mass are represented in this plane by straight lines with fixed slope, as plotted in the figure:

$$\log(\text{FWHM}) = -0.31 \log \lambda L_\lambda + 0.5 \log \frac{M_{BH}}{\text{M}_\odot} - 3.25, \qquad (2)$$

where units are the same as in equation (1). We propose that the top-right side of the triangle is the representative of a maximum mass in the quasar sample.

The third (i.e. the bottom-right) side of the triangle is supposedly due to the Eddington limit, as the loci of quasars with constant Eddington ratios are again straight lines. The dependence of FWHM on the monochromatic luminosity at a given Eddington ratio is fixed assuming the bolometric correction by Richards et al. (2006; $BC_{3000} = 5.15$) and equation (1). This yields

$$\log(\text{FWHM}) = 0.19 \log \lambda L_\lambda - 0.5 \log \frac{L_{bol}}{L_{Edd}} + 0.05, \qquad (3)$$

where units are the same as in equation (1). Note that in each redshift bin, the plotted cuts describe the shape of the quasar distribution in the FWHM–luminosity plane qualitatively well.

3.3 Construction of a probability density

Now we aim to construct a probability density of quasars as a function of FWHM and luminosity with a main criterion of simplicity. We propose that in each redshift bin the object density is only constrained by a maximum mass, a maximum Eddington ratio and a minimum luminosity due to the instrumental flux limit. We then assume a probability density of form

$$P_{l,\,\text{FWHM}}(l, \text{ FWHM}) = k \tilde{P}_l(l) \tilde{P}_m(m) \tilde{P}_e(e), \qquad (4)$$

where k is a normalization constant and each $\tilde{P}$ is assumed to be a smoothed step function, which increases from 0 to 1 (or vice versa) in a range of width σ around a fixed value of the independent variable. In the following, we describe our results assuming $\tilde{P}$ of form (see Fig. 3)

$$\tilde{P}_l(l) = \frac{1}{\sigma_l \sqrt{2\pi}} \int_{-\infty}^{l} \exp\left[-\frac{(l' - l_{\min} - 2\sigma_l)^2}{2\sigma_l^2} \right] \mathrm{d}l' \qquad (5)$$

$$\tilde{P}_m(m) = \frac{1}{\sigma_m \sqrt{2\pi}} \int_{m}^{+\infty} \exp\left[-\frac{(m' - m_{\max} + 2\sigma_m)^2}{2\sigma_m^2} \right] \mathrm{d}m' \qquad (6)$$
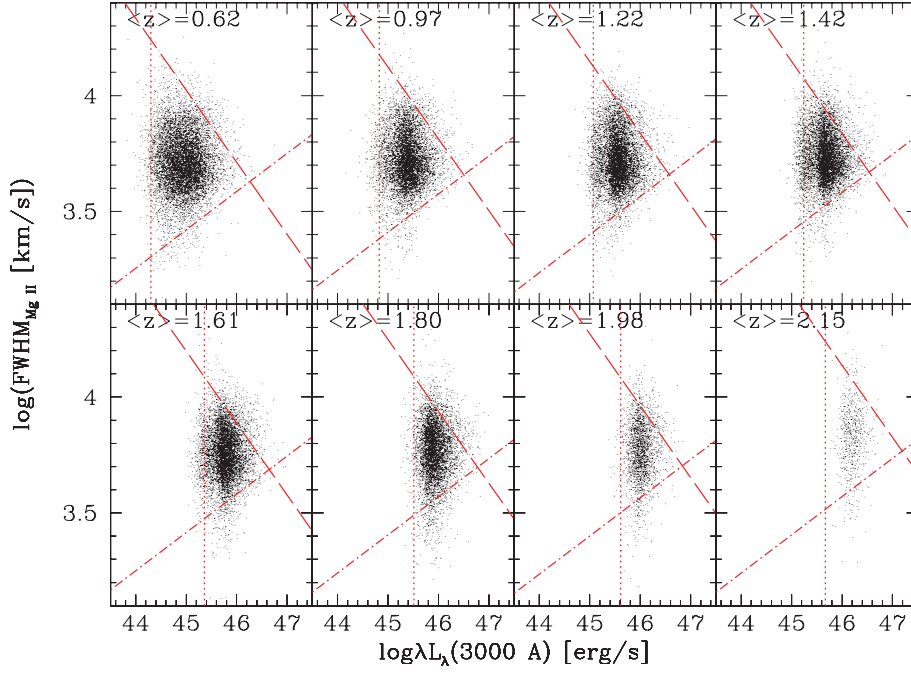
Figure 2. The eight panels show the Mg II sample in the FWHM–luminosity plane at increasing redshift. Dotted, dashed and dash–dotted lines (and lines parallel to them) represent the loci of constant monochromatic luminosity, constant mass and constant Eddington ratio, respectively.
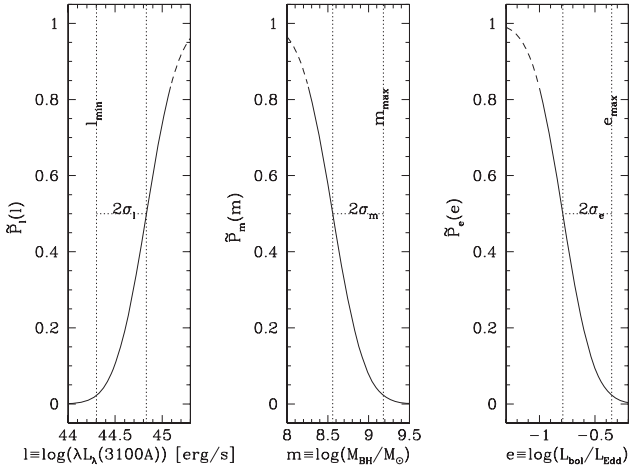

Figure 3. The shape of $\tilde{P}_l(l)$ (equation 5), $\tilde{P}_m(m)$ (equation 6) and $\tilde{P}_e(e)$ (equation 7).

$$\tilde{P}_e(e) = \frac{1}{\sigma_e\sqrt{2\pi}} \int_e^{+\infty} \exp\left[-\frac{(e'-e_{\max}+2\sigma_e)^2}{2\sigma_e^2}\right] de', \qquad (7)$$

where

$$l \equiv \log \lambda L_\lambda \qquad (8)$$

$$m = m(l, \text{FWHM}) \equiv \log \frac{M_{\text{BH}}}{\text{M}_\odot} \qquad (9)$$

$$e = e(l, \text{FWHM}) \equiv \log \frac{L_{\text{bol}}}{L_{\text{Edd}}}. \qquad (10)$$

Here, the parameters $l_{\min}$ and σ_l, $m_{\max}$ and σ_m, $e_{\max}$ and σ_e are the minimum luminosity, the maximum mass, the maximum Eddington ratio and the widths of the corresponding distributions. These

parameters will be determined in the following via a best-fitting procedure.

Note that, since the integrals of the $\tilde{P}$ functions diverge, we must restrict their domain to use them as probability densities (e.g. for values of the parameters $l \lesssim l_{\min} + 3\sigma_l$, $m \gtrsim m_{\max} - 3\sigma_m$ and $e \gtrsim e_{\max} - 3\sigma_e$). This does not significantly affect the results, because mass, Eddington ratio and luminosity are not independent variables (e.g. low-mass objects also have low luminosities or high Eddington ratios), hence the derived probability density $P_{l,\text{FWHM}}(l, \text{FWHM})$ (equation 4) is essentially insensitive to the shape of $\tilde{P}_m(m)$ at low masses, of $\tilde{P}_e(e)$ at low Eddington ratios or to the shape of $\tilde{P}_l(l)$ at high luminosities.

3.4 Best-fitting procedure

The assumed probability density depends on six free parameters, i.e. the minimum luminosity ($l_{\min}$), the maximum mass ($m_{\max}$) and Eddington ratio ($e_{\max}$) and the widths of the corresponding distributions (σ_l, σ_m and σ_e). We focus on the first redshift bin and determine the free parameters matching with the observed distribution of objects in the FWHM–luminosity plane. In detail, for each choice in the six-dimensional parameter space, the probability density has been constructed, discretized in boxes with $\Delta \log \text{FWHM} = 0.04$ dex and $\Delta \log \lambda L_\lambda = 0.2$ dex and then normalized to the total number of observed objects, in order to evaluate the expected number of objects in each box ($\Delta \log \lambda L_\lambda$, $\Delta \log \text{FWHM}$). We assumed a Poissonian error (i.e. $\sqrt{n}$) on the observed number of objects in each box. For each choice of the parameters, the expected distribution was compared to the observed distribution in the discrete $\log \lambda L_\lambda - \log \text{FWHM}$ plane, evaluating the relative χ^2 value. The minimum χ^2 determines the best-fitting parameters.

In order to determine the uncertainties on these values, the same fit procedure was repeated many times comparing the observed distribution to a set of simulated distributions of objects, constructed
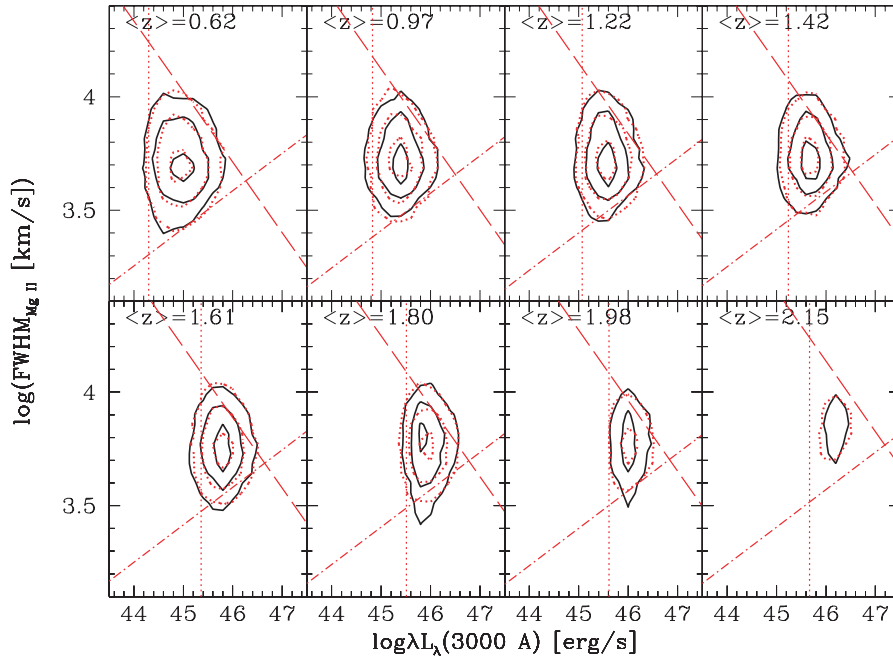
Figure 4. The eight panels show the Mg II sample in the FWHM–luminosity plane at increasing redshift: solid black contour plot (levels: 20, 90, 250 objects per box, see the text) represents the discrete observed distribution of objects. Dotted red contour plot (same levels) shows the discrete distribution of a sample of objects simulated with the Monte Carlo method, adopting the assumed $P_{l,\,\rm FWHM}(l, \rm FWHM)$ probability density with the best-fitting parameters. Dotted, dashed and dash–dotted lines represent $l_{\min}$, $m_{\max}$ and $e_{\max}$, respectively.

through the Monte Carlo method. This procedure allows an estimate of the error since we sound the underlying probability density only through a finite number of observed objects, the distribution of which in the FWHM–luminosity plane ideally follows equation (4) with a certain random dispersion. In detail, given a set of values of the six parameters, we generated 10^7 points ($\log \lambda \, L_\lambda, \log \rm FWHM$) with uniform probability densities, and then rejected points accordingly to the assumed $P_{L,\rm FWHM}(L, \rm FWHM)$ at given $l_{\min}, m_{\max}, e_{\max}$, σ_l, σ_m and σ_e, so that the number of simulated points matches the number of observed objects. We then calculated the rms between the observed and the simulated distributions. This operation was repeated for all the possible combinations of the six parameters (in a reduced phase space around the best-fitting values). The sextuple which led to the minimum rms gave the so-called Monte Carlo best-fitting parameters. This procedure was repeated a dozen times, giving as many Monte Carlo best-fitting values for each parameter, slightly different from one another, but fully consistent with the previous determination. For each parameter, the standard deviation of this set of best-fitting values was assumed as an estimate of its

uncertainty. This uncertainty is much larger than that corresponding to $\Delta \chi^2 = 1$.

In the first panel of Fig. 4, we compare the observed distribution with one simulated best-fitting distribution for the lowest redshift bin. It is apparent that the choice of three simple distributions in luminosity, mass and Eddington ratios describes the data rather closely, giving circumstantial support to the validity of the virial hypothesis on which the theoretical assumptions are based.

Table 1 (first line) contains the best-fitting values of the six parameters with relative errors and the reduced χ^2 value (χ^2_ν). The fact that the χ^2_ν is larger than 1 is interpreted as due to the choice of an oversimplified distribution. This does not influence our results, because our goal is to find a good way to quantify a parameter related to the BH mass (and one related to the Eddington ratio) such that it is not affected by a Malmquist-type bias (i.e. disentangled of the z-dependence of the luminosity instrumental limit). In fact, by construction, $m_{\max}$ and $e_{\max}$ depend neither on the quasar number density nor on the survey flux limit (see next section for tests on this statement).

Table 1. Best-fitting values of minimum luminosity, maximum mass, maximum Eddington ratio and widths of the corresponding distributions, with errors and χ^2_ν. The number of degrees of freedom is $\nu = 594$ in the first redshift bin (600 data points and six free parameters) and $\nu = 595$ in the others (600 data points and five free parameters).

Bin	$\langle z \rangle$	$l_{\min}$	σ_l	$m_{\max}$	σ_m	$e_{\max}$	σ_e	χ^2_ν
1st	0.62	**44.30 ± 0.025**	**0.26 ± 0.008**	**9.18 ± 0.05**	**0.31 ± 0.003**	**−0.35 ± 0.02**	**0.22 ± 0.003**	3.51
2nd	0.97	44.83	**0.23 ± 0.007**	**9.35 ± 0.04**	**0.31 ± 0.006**	**−0.34 ± 0.02**	**0.23 ± 0.003**	4.97
3rd	1.22	45.07	**0.23 ± 0.005**	**9.42 ± 0.05**	**0.31 ± 0.004**	**−0.33 ± 0.02**	**0.23 ± 0.002**	4.63
4th	1.42	45.24	**0.23 ± 0.008**	**9.43 ± 0.05**	**0.32 ± 0.003**	**−0.34 ± 0.02**	**0.22 ± 0.001**	5.11
5th	1.61	45.36	**0.24 ± 0.006**	**9.52 ± 0.04**	**0.31 ± 0.003**	**−0.35 ± 0.01**	**0.22 ± 0.003**	4.36
6th	1.80	45.51	**0.22 ± 0.005**	**9.60 ± 0.05**	**0.32 ± 0.002**	**−0.34 ± 0.02**	**0.22 ± 0.004**	8.44
7th	1.98	45.61	**0.22 ± 0.005**	**9.67 ± 0.05**	**0.31 ± 0.003**	**−0.33 ± 0.02**	**0.22 ± 0.004**	6.84
8th	2.15	45.67	**0.24 ± 0.006**	**10.02 ± 0.05**	**0.30 ± 0.005**	**−0.34 ± 0.02**	**0.21 ± 0.003**	7.21

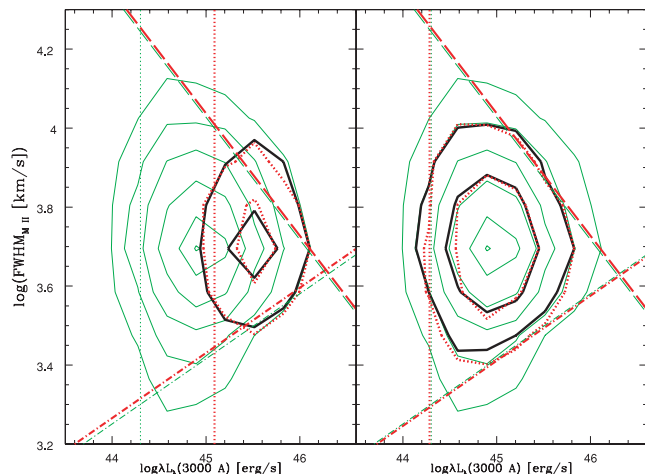*Note.* Data that come from a best-fitting procedure are displayed in bold.

Figure 5. Same as Fig. 4 referred to a subsample of the lowest redshift bin objects, selected according to the luminosity cut function of a higher redshift bin (left-hand panel) or randomly selected with $p = 0.3$ (right-hand panel). For comparison, green thin lines represent the whole low-redshift sample and its best-fitting l_{min}, m_{max} and e_{max} lines.

3.5 Bias analysis and robustness of the procedure

The effect of the luminosity cut on the results for m_{max} and e_{max} can be further tested by simulation. In order to show that our results are not affected by the instrumental flux limit of the data set, we selected a subsample from the lowest redshift bin applying the probability function $\tilde{P}_l(l)$ (equation 5) with a higher luminosity cut, i.e. assuming l_{min} and σ_1 derived for the third redshift bin in which $\langle z \rangle = 1.22$ (see next section). This subsample consists of about 1/12 of the objects in the original lowest redshift sample. The fit procedure presented in this paper has been performed again on this subsample. Fig. 5 (left-hand panel) shows that the luminosity cut of a higher redshift bin has negligible effects on the results, being these values ($m_{max} = 9.20$ and $e_{max} = -0.36$) consistent within 1σ with the best-fitting parameters derived for the whole sample ($m_{max} = 9.18 \pm 0.05$ and $e_{max} = -0.35 \pm 0.02$).

A similar test has been performed to show that m_{max} and e_{max} do not depend on the quasar number density: we resampled from the first redshift bin rejecting randomly 2/3 of the objects, in order to obtain a smaller sample with the same distribution. The fit procedure was then performed on the reduced sample. Again, no significant deviation in the determination of the best-fitting parameters was observed (see Fig. 5, right-hand panel). Again, the derived values ($m_{max} = 9.20$ and $e_{max} = -0.34$) are consistent within 1σ with the best-fitting parameters obtained for the whole sample. These tests show that m_{max} and e_{max} are independent of the quasar number density and of the survey flux limits, and therefore indicate that our procedure is not affected by a Malmquist-type bias.

4 EVOLUTION OF THE QUASI-STELLAR OBJECT POPULATION

4.1 Quasar BH mass and Eddington ratio dependence on redshift

The fit procedure described above is applied to all the redshift bins, in order to determine the best-fitting parameters and their uncertainties as a function of redshift. In each redshift bin, we compared the best-fitting minimum luminosity with the values inferred through the z-dependence of the luminosity distance (see Fig. 6). It is appar-
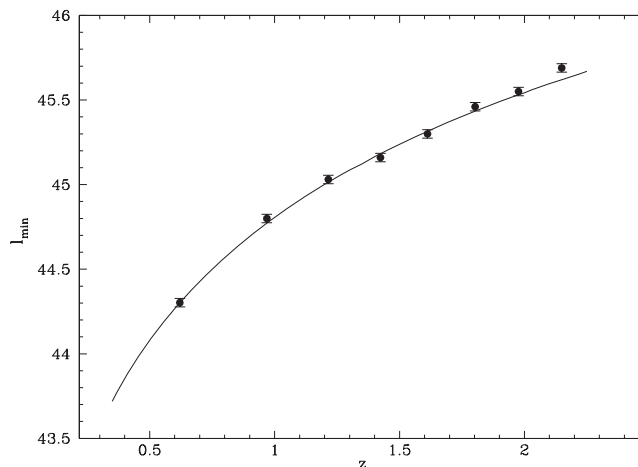

Figure 6. Black dots represent the best-fitting parameters l_{min} versus z, compared to the values expected from cosmology (solid line).

ent that the agreement is very good: apart from the highest redshift bin, where the 3000 Å continuum is very close to the red edge of the observed spectral range and the flux calibration may be unreliable, all the data are consistent with the expectations within 1σ. This gives further support to the assumed description of the object distributions in the FWHM–luminosity panels and suggests to repeat the entire procedure assuming that the value of $l_{min}(z)$ is constrained by cosmology.

The same fit procedure is then applied again to all the redshift bins, but now the dependence on redshift of the minimum luminosity is set by cosmology and l_{min} is no more treated as a free parameter. In each bin, the χ^2_ν was evaluated and normalized to the $\chi^2_{\nu 0}$ value obtained in the first redshift bin, in order to compare the adequacy of the best-fitting function in the eight panels. Fig. 7 shows that these values are almost constant in each redshift bin. Again, Fig. 4 and Table 1 show, respectively, the Monte Carlo simulated distributions compared to the observed distributions of quasars and the best-fitting values, their errors and relative χ^2 values.

The maximum mass and Eddington ratio values are plotted versus redshift in Fig. 8. Note that the proposed M_{BH} z-dependence refers
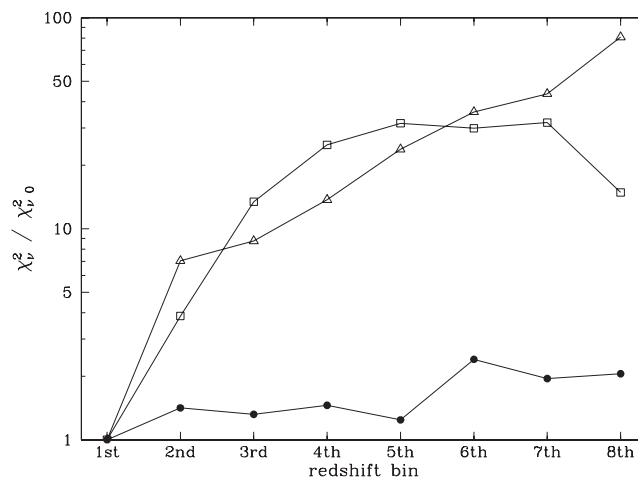

Figure 7. Normalized χ^2_ν values of the best-fitting function. Filled circles refer to the fit procedure described in this work. Open triangles show the χ^2_ν values that would be obtained assuming that the quasar BH mass is constant with redshift, and open squares show the χ^2_ν values assuming that the BH mass evolves with redshift as proposed by Fine et al. (2006).
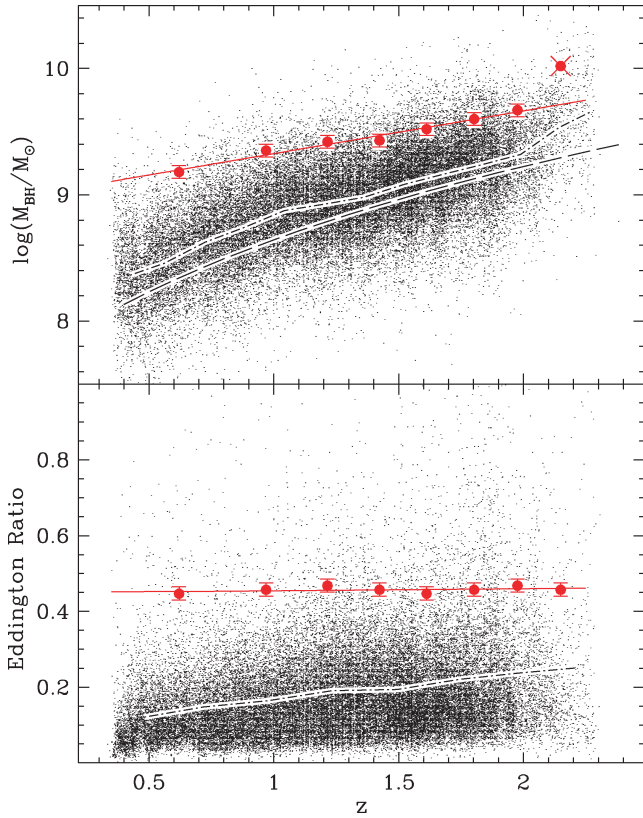
Figure 8. Upper panel: small dots are the virial BH masses of the Mg II sample given by Shen et al. (2008); the dash–dotted line reports the corresponding mean values. Red circles are our estimates of $\log \frac{M_{BH(max)}}{M_\odot}$ and the red solid line is the best fit reported in equation (11). The M_{BH} versus z-dependence proposed by Fine et al. (2006) is the dashed line. Lower panel: small dots are the Eddington ratios for each source of the Mg II sample; the dash–dotted line shows the corresponding average. Red circles are the maximum Eddington ratios and the red solid line is the best linear fit reported in equation (12).

to the active BH population and not to the total supermassive BH mass distribution. Of course, the average mass of the inactive BH population must decrease with increasing redshift.

A linear fit to the maximum mass values (excluded the highest redshift bin one) gives

$$\log \frac{M_{BH(max)}}{M_\odot} = m_{max} = 0.34(\pm 0.02)z + 8.99(\pm 0.03); \quad (11)$$

while the maximum Eddington ratio (~ 0.45) is consistent with no evolution with cosmic time

$$\frac{L_{bol}}{L_{Edd}}(max) = 10^{(e_{max})} = 0.005(\pm 0.006)z + 0.45(\pm 0.01). \quad (12)$$

Assuming that the shapes of M_{BH} and Eddington ratio distributions do not change with redshift, which is suggested by the fact that the value of σ_m and σ_e is independent of z (see Table 1), equation (11) also describes the slope of the z-dependence of the mean quasar BH mass, and not only of the maximum mass of the quasar populations. Similarly, the mean (and not only the maximum) Eddington ratio is constant with redshift.

4.2 Dependence of the results on the $r_{BLR} - \lambda L_\lambda$ calibration

We tested whether a variation of the luminosity exponent of the virial calibration may affect the relative evolution in m_{max} and e_{max}
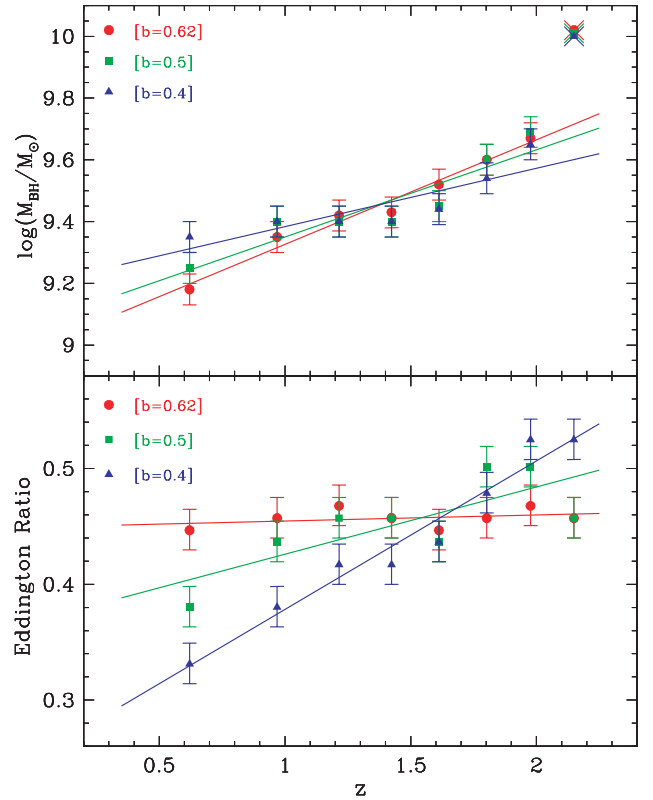

Figure 9. BH maximum masses (upper panel) and maximum Eddington ratios (lower panel) as a function of redshift for different values of the luminosity exponent in equation (1).

derived in this paper. The $L - r_{BLR}$ relation assumed in equation (1) (McLure & Dunlop 2004) is quite steep, although still consistent with the canonical $r_{BLR} \propto \lambda L_\lambda^b$ with $b = 0.5$ which is often assumed for idealized photoionization. In order to quantify the effects that this has on the relative evolution in the maximum mass and Eddington ratio, we reproduced the analysis assuming the exponent on the luminosity term is $b = 0.5$ or 0.4, both of which are consistent to within 2σ with the McLure & Dunlop (2004) calibration in which $b = 0.62 \pm 0.14$.

Fig. 9 (upper panel) shows that the smaller is the luminosity exponent in the virial calibration, the flatter is the dependence on redshift of the BH masses. The results are only slightly affected by the choice of the $L - r_{BLR}$ relation, since the z-evolution determined assuming an exponent of 0.5 is consistent within 1σ with the previous determination, obtained assuming the McLure & Dunlop (2004) virial calibration. In Table 2, we give the best linear fit to the maximum mass as a function of redshift for $b = 0.5$, 0.4 and, for comparison, $b = 0.62$.

On the other hand, with regards to the dependence on redshift of the Eddington ratio, the picture is more delicate. This parameter appears to increase significantly with z assuming a flatter $L - r_{BLR}$ relation, while it was found to be constant with redshift within the assumed virial calibration (equation 1; see Fig. 9, lower panel). In Table 2, the parameters of the best linear fit to the maximum Eddington ratio as a function of redshift are given for various values of the luminosity exponent ($b = 0.5$, 0.4 and, for comparison, $b = 0.62$).

Note that the assumption of a flatter $L - r_{BLR}$ relation leads to an increase of the residuals between the best-fitting probability density (equation 4) and the observed quasar distribution. In Table 2, the

Table 2. Best linear fit to the maximum mass and to the maximum Eddington ratio as a function of redshift for various values of the luminosity exponent in equation (1) ($b = 0.62$, 0.5 and 0.4). For each value of b, the average value over all the redshift bins of the χ_ν^2 of the best-fitting probability density (equation 4) is also given.

b	$\log \frac{M_{\mathrm{BH(max)}}}{M_\odot} = \alpha z + \beta$		$\frac{L_{\mathrm{bol}}}{L_{\mathrm{Edd}}} (\mathrm{max}) = \alpha z + \beta$		$\langle \chi_\nu^2 \rangle_z$
	α	β	α	β	
0.62	0.34 ± 0.02	8.99 ± 0.03	0.005 ± 0.006	0.45 ± 0.01	5.6
0.5	0.28 ± 0.05	9.07 ± 0.08	0.06 ± 0.02	0.37 ± 0.03	5.8
0.4	0.19 ± 0.05	9.19 ± 0.07	0.13 ± 0.01	0.25 ± 0.02	7.5

χ_ν^2 values averaged over z of the best-fitting probability density are given for $b = 0.62$, 0.5 and 0.4. It is apparent that the χ_ν^2 is minimum for $b = 0.62$, giving a circumstantial independent support to the index proposed by McLure & Dunlop (2004, see equation 1) and, hence, to equations (11) and (12).

4.3 Comparison with previous results

We now compare our results with those obtained by McLure & Dunlop (2004), Fine et al. (2006) and Shen et al. (2008), focusing just on the slope of the M_{BH} and Eddington ratio evolution.

Fine et al. (2006), in order to reduce the effects of the Malmquist bias, concentrated on a subsample of the 2dF quasars with luminosity around $L^*(z)$ at each redshift. They observe a significant dependence of the quasar BH mass on redshift [$M_{\mathrm{BH}} \propto (1 + z)^{3.3 \pm 1.1}$], but conclude that their result cannot directly be interpreted as evidence for antihierarchical 'downsizing' because the z-dependence they found is strongly dominated by the dependence on redshift of L^*. For comparison, we repeated the entire fit procedure described above imposing that $M_{\mathrm{BH(max)}}(z)$ varied as proposed by Fine et al. (2006). Fig. 7 shows the relative χ_ν^2 values in each redshift bin: the fit appears inadequate if we assume their results. Note however that the error given for the evolution of the average BH mass of QSOs by Fine et al. (2006) is quite large, so that their results are consistent with those given here within 1σ.

McLure & Dunlop (2004) proposed that the observed increase of the quasar BH mass with redshift is entirely as expected due to the effective flux limit of the sample. To further test the possibility that the mean BH mass is independent of redshift, we again repeated the fit procedure described above assuming that $M_{\mathrm{BH(max)}}$ is constant over all the redshift bins. In Fig. 7, we plot the relative χ_ν^2, and again the fit is inconsistent with the data, giving further evidence for an evolution of quasar populations with z.

McLure & Dunlop (2004) and Shen et al. (2008), studying the SDSS DR1 and DR5 samples, found that there is a clear upper mass limit of $\sim 10^{10} \, M_\odot$ for active BHs at $z > 2$, decreasing at lower redshift. This trend is in good agreement with our results and can be explained assuming that the quasar number density peaks at a certain $z_{\mathrm{peak}} \sim 2$–2.5 and then flattens out (see e.g. Richards et al. 2006a). Around z_{peak}, both the high- and the low-mass end of the quasar BH mass distribution are more populated, so that the observation of very massive objects is likely (while low-mass quasars cannot be observed due to the instrumental flux limit). Therefore, the slope of the 'unbiased' dependence on redshift of the maximum BH mass is raised below z_{peak} and it is flattened above. This effect translates in evidence for a limiting BH mass for active BHs at $z > 2$, decreasing at lower redshift, that is apparent in all large samples of quasars.

McLure & Dunlop (2004) observed a substantial increase of Eddington ratios with redshift and a similar trend is apparent from the sample of 2dF L^* quasars of Fine et al. (2006) after correcting

their data for the offset between the Mg II and C IV virial mass calibrations (see e.g. Shen et al. 2008). We suggest that the observed z-dependence of Eddington ratios is spurious, and that it is entirely dominated by the dependence on redshift of the average quasar luminosity due to the Malmquist bias.

4.4 Discussion of the results

Studying a sample of $\sim 50\,000$ SDSS quasars with $0.35 < z < 2.25$, we obtained that the maximum mass of the quasar populations increases with z, while the maximum Eddington ratio is practically independent of redshift.

These results are unaffected by the Malmquist bias and may be interpreted as evidence for evolution of the active BH population with redshift. Quasar samples at lower redshift are increasingly dominated by lower mass BHs, i.e. most massive BHs start quasar activity before less massive ones. This is indicative of antihierarchical 'downsizing' of active BHs, and it is in agreement with recent theoretical predictions by e.g. Merloni, Rudnick & Di Matteo (2008).

Our findings may have implications for the study of the co-evolution of supermassive BHs and their host galaxies, even if they cannot be directly interpreted as evidence for evolution of the $M_{\mathrm{BH}} - M_{\mathrm{bulge}}$ scale relation. There is observational evidence that quasar host galaxies are already fully formed massive ellipticals at $z \sim 2.5$ and then passively fade in luminosity to the present epoch (e.g. Kotilainen et al. 2007, 2009; Falomo et al. 2008). Within this scenario, our results can be interpreted as an evolution with redshift of the parameter $\Gamma \equiv M_{\mathrm{BH}}/M_{\mathrm{bulge}}$, which would be four to five times larger at $z \sim 2$ than today.

This is in good agreement with the results of Peng et al. (2006), who found that Γ is ~ 4 times larger at $z \sim 1.7$ than today in a sample of 11 lensed quasar hosts. Our results are also consistent with Salviander et al. (2007), who examined a sample of SDSS quasars finding that galaxies of a given dispersion at $z \sim 1$ have BH masses that are larger by $\Delta \log M_{\mathrm{BH}} \sim 0.2$ than at $z \sim 0$ (see Lauer et al. 2007 for a detailed discussion on the selection bias which may affect these results).

5 SUMMARY AND CONCLUSIONS

Starting from the SDSS DR5 quasar catalogue, we focused on the $\sim 50\,000$ objects for which Mg II line widths and 3000 Å monochromatic luminosities were available. This sample ($0.35 < z < 2.25$) was divided in eight redshift bins. In each bin, the object distribution in the FWHM–luminosity plane was described in terms of a minimum luminosity limit (due to the instrumental flux limit), a maximum mass and a maximum Eddington ratio. The assumed probability density was compared to the observed distribution of objects in order to determine the free parameters with a best-fitting

procedure in each redshift bin. Errors on the best-fitting parameters were determined with Monte Carlo simulations.

We tested the robustness of the procedure through some simulations, and showed that the maximum mass and the maximum Eddington ratio determined in each redshift bin depend neither on the quasar number density nor on the survey flux limit (which is responsible for giving rise to a Malmquist-type bias in the observed dependence on redshift of the mean quasar BH masses).

We then studied the dependence on redshift of the maximum quasar BH mass and of the maximum Eddington ratio and found clear evidence for evolution of the active BH population with redshift. Over the redshift range studied, we obtained that the maximum mass of the quasar population depends on redshift as $\log [M_{BH(max)}/M_\odot] = 0.34z + 8.99$, while the maximum Eddington ratio is found to be practically independent of redshift.

This means that QSO samples at lower redshift are increasingly dominated by lower mass BHs, i.e. the more massive a BH is, the earlier it starts quasar activity. Within a scenario in which quasar host galaxies are already fully formed massive ellipticals at $z \sim 2.5$, our results can also be interpreted as an evolution with redshift of the parameter $\Gamma \equiv M_{BH}/M_{bulge}$, which would be four to five times larger at $z \sim 2$ than today.

ACKNOWLEDGMENTS

REFERENCES

Croom S. M., Smith R. J., Boyle B. J., Shanks T., Miller L., Outram P. J., Loaring N. S., 2004, MNRAS, 349, 1397

Falomo R., Treves A., Kotilainen J. K., Scarpa R., Uslenghi M., 2008, ApJ, 673, 694

Fine S. et al., 2006, MNRAS, 373, 613

Fine S. et al., 2008, MNRAS, 390, 1413

Kotilainen J. K., Falomo R., Labita M., Treves A., Uslenghi M., 2007, ApJ, 660, 1039

Kotilainen J. K., Falomo R., Decarli R., Treves A., Uslenghi M., Scarpa R., 2009, ApJ, in press

Lauer T. R., Tremaine S., Richstone D., Faber S. M., 2007, ApJ, 670, 249

McLure R. J., Dunlop J. S., 2004, MNRAS, 352, 1390

Merloni A., Rudnick G., Di Matteo T., 2008, in Aschenbach B., Burwitz V., Hasinger G., Leibundgut B., eds, Proc. MPE/USM/MPA/ESO Joint Astron. Conf., ESO Astrophys. Symp., Relativistic Astrophysics Legacy and Cosmology. Springer, Berlin, p. 158

Peng C. Y., Impey C. D., Rix H.-W., Kochanek C. S., Keeton C. R., Falco E. E., Lehár J., McLeod B. A., 2006, ApJ, 649, 616

Richards G. T. et al., 2006a, ApJS, 166, 470

Richards G. T. et al., 2006b, AJ, 131, 2766

Salviander S., Shields G. A., Gebhardt K., Bonning E. W., 2007, ApJ, 622, 131

Schneider D. P. et al., 2007, AJ, 134, 102

Shen Y., Greene J. E., Strauss M. A., Richards G. T., Schneider D. P., 2008, ApJ, 680, 169

Vestergaard M., Fan X., Tremonti C. A., Osmer P. S., Richards G. T., 2008, ApJ, 674, L1

This paper has been typeset from a TEX/LATEX file prepared by the author.